Determination of Sr properties for a high-accuracy optical clock

S. G. Porsev,[1,2,*] Andrew D. Ludlow,[1,†] Martin M. Boyd,[1] and Jun Ye[1]

[1]*JILA, National Institute of Standards and Technology and University of Colorado,*
Department of Physics, University of Colorado, Boulder, Colorado 80309-0440, USA
[2]*Petersburg Nuclear Physics Institute, Gatchina, Leningrad district, 188300, Russia*

We have carried out calculations towards the goal of reducing the inaccuracy of the Sr optical atomic clock to 1×10^{-17} and below. In particular, we focused on ac polarizabilities of the $5s^2\ ^1S_0$ and $5s5p\ ^3P_0^o$ clock states that are important for reducing the uncertainty of black-body radiation-induced frequency shifts for the $^1S_0$-$^3P_0^o$ clock transition. Four low-lying even-parity states have been identified, whose total contribution to the static polarizability of the $^3P_0^o$ clock state is at the level of 90%. We show that if the contribution of these states is experimentally known with 0.1% accuracy, the same accuracy can be achieved for the total polarizability of the $^3P_0^o$ state. The corresponding uncertainty for the blackbody shift at a fixed room temperature will be below 1×10^{-17}. The calculations are confirmed by a number of experimental measurements on various Sr properties.

PACS number(s): 31.15.ac, 31.15.am, 31.15.ap, 32.70.Cs

I. INTRODUCTION

The use of optical lattice-confined neutral atoms for achieving a new level of time-keeping precision and accuracy has become widely practiced (see, e.g., Refs. [1–9]). In this scheme, ultracold atoms are confined in an optical lattice to eliminate motion-related systematic frequency shifts. The lattice laser wavelength is selected in such a way that the perturbation to the clock frequency arising from ac Stark shifts induced by the lattice laser for both clock states exactly cancel [10].

An important indicator of clock performance is provided by the Allan deviation characterizing the fractional frequency instability σ. For a signal-to-noise ratio given by the fundamental quantum projection noise, the instability can be written as

$$\sigma(\tau) \simeq \frac{1}{Q} \frac{\sqrt{t}}{\sqrt{N\tau}}. \tag{1}$$

Here Q is the resonance quality factor defined as $Q = \nu/\Delta\nu$, where ν is the transition frequency and $\Delta\nu$ is the linewidth. N is the total number of particles measured in a coherent time period t, and τ is the total averaging time. According to Eq. (1), atoms with the highest quality factors Q are preferred for a new generation of time and frequency standards.

The highest Q's are currently obtained for a narrow transition in the optical domain [11]. In particular, the highly forbidden $^1S_0 \rightarrow {}^3P_0^o$ transitions in divalent atoms offer excellent possibilities for attaining a new level of precision and accuracy for time keeping. One of the most promising candidates is ^{87}Sr for which $\Delta\nu \approx 1.2$ mHz [12–14], yielding a potential $Q > 10^{17}$. In a recent paper [8], a systematic uncertainty evaluation for a neutral Sr optical atomic standard was reported at the 10^{-16} fractional level, surpassing the best

evaluations of Cs fountain primary standards. The dominant systematic frequency correction and uncertainty in that work arose from the room temperature black-body radiation (BBR). The fractional frequency shift $|\delta\nu_{\text{BBR}}/\nu_0|$ caused by the BBR is proportional to the differential static polarizability of the two clock states. For the $5s^2\ ^1S_0 \rightarrow 5s5p\ ^3P_0^o$ transition in Sr, the BBR shift was calculated in Ref. [15] to be equal to $55.0(7) \times 10^{-16}$. The 1% uncertainty for the BBR shift originates mostly from insufficient knowledge of the static polarizability of the $5s5p\ ^3P_0^o$ state, with the most accurate calculation provided in Ref. [15]. To further improve the Sr accuracy, it is clear that a better understanding of the Sr properties is needed to give a more accurate determination of the BBR shift. The purpose of this paper is to outline a clear path to achieve this goal. To improve the clock accuracy significantly, it is equally important that a well-characterized homogeneous BBR environment surrounds the Sr atoms in future experiments.

The improvement of the Sr clock accuracy requires a more accurate determination of the differential static polarizability of the $5s^2\ ^1S_0$ and $5s5p\ ^3P_0^o$ states. Note that the static polarizability of the ground $5s^2\ ^1S_0$ state is known at a sufficiently low uncertainty $\sim 0.1\%$ [15]. This low uncertainty is made possible by a good knowledge of the matrix element $|\langle 5s^2\ ^1S_0 \| d \| 5s5p\ ^1P_1^o \rangle|$ [16], where the intermediate state $5s5p\ ^1P_1^o$ contributes to the polarizability of the $^1S_0$ state at the dominant level of 97%. Consequently, the outstanding challenge is to reduce the uncertainty of the polarizability of the $^3P_0^o$ state to a similar level. Even sophisticated modern relativistic methods of atomic calculations cannot provide such accuracy. For this reason, a solution to this problem must combine theoretical and experimental approaches. We show that four specific intermediate states have a combined contribution to the total static polarizability of the $5s5p\ ^3P_0^o$ state at the level of 90%. When the contributions from these four states are determined from experimental data at 0.1% accuracy and the contributions of all other discrete and continuum states are known at the level of 1–2 % from calculations, then the final 0.1% uncertainty for the polarizability of the $5s5p\ ^3P_0^o$ state will be achieved. This strategy is the focus of this paper.

*sporsev@gmail.com
†Present address: NIST Time and Frequency Division, Boulder, Colorado, 80309, USA.

The paper is organized as follows. In Sec. II we briefly describe the method of calculations. In particular, we discuss the construction of basis sets and solving the multiparticle Schrödinger equation. In Sec. III we discuss the black-body radiation effect and present the results of calculations for the low-lying energy levels, ac polarizabilities, transition rates, and oscillator strengths, and we analyze the results obtained. Section IV contains concluding remarks. Atomic units ($\hbar = |e| = m = 1$) are used throughout the paper.

II. METHOD OF CALCULATIONS

The most complex problem in precise atomic calculations is associated with the necessity to account for three types of electron correlations, i.e., valence-valence, core-valence, and core-core correlations. The former are usually too strong to be treated perturbatively, while the other two types of correlations cannot be treated effectively with nonperturbative techniques, such as the multiconfigurational Hartree-Fock method [17] or the configuration interaction (CI) method [18,19].

Therefore, it is natural to combine the many-body perturbation theory (MBPT) with one of the nonperturbative methods. In Ref. [20], it was suggested to use MBPT in order to construct an effective Hamiltonian for valence electrons. After that, the multiparticle Schrödinger equation for valence electrons is solved within the CI framework. Doing so allows us to find the low-lying energy levels. Following the earlier works, we refer to this approach as the CI+MBPT formalism.

In order to calculate other atomic observables, one has to construct the corresponding effective operators for valence electrons [21–23]. These operators effectively account for the core-valence and core-core correlations. In particular, to obtain an effective electric-dipole operator, we solve random-phase approximation (RPA) equations, thus summing a certain sequence of many-body diagrams to all orders of MBPT [21,24,25]. The RPA describes shielding of an externally applied field by core electrons. Small corrections due to, for instance, normalization and structural radiation are omitted.

In the CI+MBPT approach, the energies and wave functions are determined from the time-independent Schrödinger equation

$$H_{\text{eff}}(E_n)\Phi_n = E_n\Phi_n,$$

where the effective Hamiltonian is defined as

$$H_{\text{eff}}(E) = H_{\text{FC}} + \Sigma(E).$$

Here H_{FC} is the Hamiltonian in the frozen core approximation and Σ is the energy-dependent correction, which takes into account virtual core excitations. The operator Σ completely accounts for the second-order perturbation theory over residual Coulomb interactions. Determination of the second-order corrections requires calculation of one- and two-electron diagrams. The one-electron diagrams describe an attraction of a valence electron by a (self-) induced core polarization. The two-electron diagrams are specific for atoms with several valence electrons. The number of the two-electron diagrams is very large and their calculations are extremely time-consuming. In the higher orders the calculation of two-electron diagrams becomes practically impossible. Hence, it is more promising to account for the high orders of the MBPT indirectly. One such method was suggested in Ref. [26], where it was shown that a proper choice of the optimum initial approximation for the effective Hamiltonian can substantially improve the agreement between calculated and experimental spectra of many-electron atoms.

We consider Sr as a two-electron atom with the core $[1s, \ldots, 4p^6]$. The one-electron basis set for Sr includes $1s$-$14s$, $2p$-$14p$, $3d$-$13d$, $4f$-$13f$, and $5g$-$9g$ orbitals, where the core- and $5s$-$7s$, $5p$-$7p$, and $4d$-$6d$ orbitals are Dirac-Hartree-Fock (DHF) ones and all the rest are the virtual orbitals. The orbitals $1s$-$5s$ were constructed by solving the DHF equations in the V^N approximation, i.e., the core and the $5s$ orbitals were obtained from the DHF equations for a neutral atom (we used the DHF computer code [27]). The $6s$-$7s$, $5p$-$7p$, and $4d$-$6d$ orbitals were obtained in the V^{N-1} approximation. That is, the $1s$-$5s$ orbitals were "frozen," one electron was transferred from the valence $5s$ shell into one of the orbitals specified above, and the corresponding one-electron wave function was found by solving the DHF equations. We determined virtual orbitals using a recurrent procedure similar to Ref. [28] and described in detail in Refs. [22,23].

Configuration-interaction states were formed using these one-particle basis sets. It is worth emphasizing that the employed basis set was sufficiently large to obtain numerically converged CI results. An extended basis set, used at the stage of MBPT calculations, included $1s$-$21s$, $2p$-$21p$, $3d$-$20d$, $4f$-$17f$, and $5g$-$13g$ orbitals.

III. RESULTS AND DISCUSSION

A. Calculation of energies

Solving the multiparticle Schrödinger equation we find low-lying energy levels and their respective wave functions. In Table I we present the calculated energies of the low-lying states for Sr and compare them with experimental data. As is seen from the table we focus mainly on energy levels with $J=1$. This is due to the fact that we are interested in calculation of the electric dipole-dominated ac polarizabilities for the clock states with total angular momentum $J=0$. Only intermediate states with $J=1$ contribute to these polarizabilities. The energy level diagram of these states is given in Fig. 1. The energy levels were obtained in the framework of the conventional configuration-interaction method as well as using the formalism of CI combined with the many-body perturbation theory. Using the CI method alone, the agreement of the calculated and experimental energies is at the level of 5–10 %. The combination of CI and MBPT improves the accuracy by approximately an order of magnitude.

B. Black-body radiation

It is well known that BBR-related clock frequency shifts arise from perturbations of atomic energy levels by weakly oscillating thermal radiation. For the $^1S_0 \rightarrow {}^3P_0^o$ clock transi-

TABLE I. Energy differences (in cm^{-1}) with respect to the ground $5s^2$ $^1S_0$ state for the low-lying energy levels of Sr.

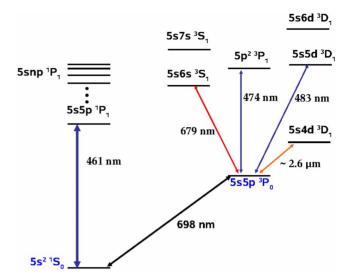| Config.	Level	CI	CI+MBPT	Experiment [29]
$5s4d$	$^3D_1$	19 571	18 076	18 159
$5s4d$	$^3D_2$	19 587	18 141	18 219
$5s4d$	$^3D_3$	19 617	18 254	18 319
$5s4d$	$^1D_2$	20 166	19 968	20 150
$5s6s$	$^3S_1$	27 488	29 019	29 039
$5s5d$	$^3D_1$	33 358	35 060	35 007
$5p^2$	$^3P_1$	33 511	35 326	35 194
$5s7s$	$^3S_1$	35 695	37 429	37 425
$5s6d$	$^3D_1$	37 985	39 725	39 686
$5s5p$	$^3P_0^o$	12 490	14 241	14 317
$5s5p$	$^3P_1^o$	12 663	14 448	14 504
$5s5p$	$^3P_2^o$	13 022	14 825	14 899
$5s5p$	$^1P_1^o$	20 832	21 469	21 698
$5s6p$	$^3P_1^o$	32 110	33 814	33 868
$5s6p$	$^1P_1^o$	32 487	34 105	34 098
$4d5p$	$^3D_1^o$	36 699	36 189	36 264
$4d5p$	$^3P_1^o$	36 944	37 213	37 303
$5s7p$	$^1P_1^o$	37 275	38 927	38 907
$5s7p$	$^3P_1^o$	37 939	39 377	39 427

FIG. 1. (Color online) Low-lying energy levels and transition wavelengths of atomic Sr, relevant for the determination of polarizabilities of the $5s^2$ $^1S_0$ and $5s5p$ $^3P_0^o$ clock states.

tion, both atomic states involved are perturbed. Thus, the net BBR effect is the difference of the individual BBR shifts for the two states, $\delta\omega_{BBR} = \delta E_{BBR}(^3P_0^o) - \delta E_{BBR}(^1S_0)$. The expression for the $\delta E_{BBR}(g)$ of a state g can be given by the following formula [15]:

$$\delta E_{BBR}(g) = -\frac{2}{15}(\alpha\pi)^3 T^4 \alpha_{E_g}(0)[1+\eta], \qquad (2)$$

where $\alpha \approx 1/137$ is the fine structure constant, T is the characteristic temperature of the BBR environment, $\alpha_{E_g}(0)$ is the electric-dipole static polarizability of state g, and η represents a "dynamic" fractional correction to the total shift. As was shown in Ref. [15], η is negligible for the $^1S_0$ state but contributes to δE_{BBR} of the $^3P_0^o$ state at the 2.7% level. This is primarily due to the fact that the $^3P_0^o$ state has a transition to a nearby $5s4d$ $^3D_1$ state in the infrared, as shown in Fig. 1.

The electric dipole static polarizabilities of the $5s^2$ $^1S_0$ and $5s5p$ $^3P_0^o$ states were calculated in Ref. [15] using the same method, but employing a different basis set than is presented in this work. The corresponding relative frequency shift of the clock transition was determined to be $|\delta\nu_{BBR}/\nu_0| = 55.0(7) \times 10^{-16}$. The shift uncertainty of $\Delta[\delta\nu_{BBR}/\nu_0] = 0.7 \times 10^{-16}$ results directly from the 1% uncertainty attained in Ref. [15] for the static polarizability $\Delta[\alpha_{^3P_0^o}(0)]$ of the $5s5p$ $^3P_0^o$ state. The small size of η ensured that no additional uncertainty from the dynamical correction contributed at this level.

An equally important source of uncertainty in the actual BBR shift is the knowledge and control of the blackbody environment at room temperature, T. From Eq. (2), the shift uncertainty $\Delta[\delta E_{BBR}(g)]$ originating from the uncertainty in the BBR environment ΔT is

$$\Delta[\delta E_{BBR}(g)] = -\frac{8}{15}(\alpha\pi)^3 T^3 \alpha_{E_g}(0)[1+\eta]\Delta T. \qquad (3)$$

At room temperature, measurement of the BBR environment at the uncertainty level of $\Delta T = 1$ K leads to a fractional frequency shift uncertainty of 7.5×10^{-17} [8]. The combination of this uncertainty in quadrature with that resulting from $\Delta[\alpha_{^3P_0^o}(0)]$ yields a 1×10^{-16} total BBR uncertainty, which currently limits the accuracy of the Sr optical clock.

To further improve the Sr accuracy, the total BBR uncertainty must be reduced. This requires solving two main problems: (i) measuring and controlling the black-body environment to much better than $\Delta T = 1$ K; (ii) determining the differential static polarizability to better than 1% uncertainty. The first of these requires additional care and design in the experimental apparatus. While the temporal stability of the BBR temperature is more or less straightforward to achieve, the experimental difficulty originates from achieving spatial homogeneity of the BBR temperature over various functional areas of the vacuum chamber housing the atomic sample. Typically, a large fraction of the 4π sterradians of solid angle around the atoms consists of glass viewports to accommodate the optical access needed for various atomic manipulations (laser cooling and trapping, loading into an optical lattice, state preparation, etc.). These areas are more difficult to precisely temperature stabilize than the remainder of the solid angle typically composed of a metallic vacuum chamber. Experimentally, we observe that different parts of the Sr vacuum apparatus at JILA can vary by as much as 1 K. Furthermore, at the highest clock accuracy level, it is important to account for the effect of the transmissivity of glass viewports for visible and infrared radiation from the ambient room on the blackbody environment seen by the atoms.

One approach to reducing the uncertainty of the BBR shift is to surround the atomic sample in a cryogenically cooled shield [30]. Doing so reduces both the magnitude and thus the uncertainty of the BBR shift. Another approach is to enclose the atoms in a chamber closely resembling the black-body cavities used for thermal radiation metrological standards [31]. For example, the optically confined atoms can be transported in a moving lattice from a main chamber to a smaller, black-body cavity [8]. By careful temperature control of this small cavity made of highly-thermally conductive material, excellent temperature homogeneity can be maintained. The very limited optical access (for lattice laser and clock probes) enables the effective emissivity of the cavity interior to be very close to unity. To reach the 10^{-17} clock uncertainty, the BBR environment must be known at the part per thousand level at room temperature, corresponding to a BBR temperature accuracy at the 100 mK level.

The differential polarizability must also be carefully determined to higher accuracy. In the case of cesium, a well-controlled dc electric field has been used to induce a clock shift and determine the differential static polarizability [32]. As well, some atom interferometric techniques may hold promise for directly measuring the differential polarizability at better than the 1% level [33]. Here we address the improved determination of the differential polarizability based on atomic structure measurements. The uncertainty of the differential static polarizability is determined by the uncertainties in the polarizabilities of the two clock states. The static polarizability of the ground state $\alpha_{^1S_0}(0)$ $=197.2(2)$ a.u. [15] is known with 0.1% accuracy. Consequently, the task at hand is to determine the static polarizability of the $5s5p\ ^3P_0^o$ state with a similar level of accuracy. This is a key step towards Sr lattice clock operation at the 10^{-17} uncertainty level. We now discuss this problem in detail and present a possible solution in the following sections.

C. Calculation of electric dipole ac polarizabilities of the $5s^2$ $^1S_0$ and $5s5p\ ^3P_0^o$ states

Using the wave functions of the low-lying states obtained as a result of solving the multiparticle Schrödinger equation, we are able to calculate ac polarizabilities of the $5s^2\ ^1S_0$ and the $5s5p\ ^3P_J^o$ states. As one check of the quality of our calculations, we can find the magic wavelengths: λ_0 at which $\alpha_{^1S_0}(\lambda_0)=\alpha_{^3P_0^o}(\lambda_0)$ and λ_1 at which $\alpha_{^1S_0}(\lambda_1)=\alpha_{^3P_1^o}(\lambda_1)$ and compare these values against the experimental results. In recent works these magic wavelengths were determined with high precision to be $\lambda_0(^1S_0-{}^3P_0^o)=813.42735(40)$ nm [8] and $\lambda_1(^1S_0-{}^3P_1^o(m_J=\pm 1))=914(1)$ nm for linear polarization [34]. Furthermore, our calculation can also be checked against a recent measurement of the ac Stark shift associated with the probe of the $(^1S_0\rightarrow {}^3P_0^o)$ clock transition itself [8].

We start with a brief description of the method used to calculate the electric dipole polarizabilities. The equation for the ac electric dipole polarizability of a state g can be written in the following form:

$$\alpha_{E_g}(\omega) = 2\sum_k \frac{(E_k-E_g)|\langle g|d_0|k\rangle|^2}{(E_k-E_g)^2-\omega^2}$$

$$= \sum_k \frac{|\langle g|d_0|k\rangle|^2}{E_k-(E_g+\omega)} + \sum_k \frac{|\langle g|d_0|k\rangle|^2}{E_k-(E_g-\omega)}$$

$$\equiv \frac{1}{2}\{\alpha_{E_g+\omega}(0) + \alpha_{E_g-\omega}(0)\}. \quad (4)$$

The two terms in the bottom line of Eq. (4) can be viewed as the static polarizabilities of state g calculated for the shifted energy levels of $E_g+\omega$ and $E_g-\omega$, respectively. Thus, our task is reduced to computation of these two static polarizabilities.

Following Refs. [35,36] we decompose an ac polarizability into two parts

$$\alpha(\omega) = \alpha^v(\omega) + \alpha^c(\omega). \quad (5)$$

The first term describes excitations of the valence electrons. The second term characterizes excitations of core electrons and includes a small counter term related to excitations of core electrons to occupied valence state. The core polarizability α^c was calculated at $\omega=0$ to be $\alpha^c(0)=5.4$ a.u. [15]. Since α^c contributes to the total polarizability only at the level of a few percent and its dependence on frequency is very weak, the value of 5.4 a.u. can also be used for calculations of the total ac polarizabilities. This approximation of a constant core polarizability over the relevant frequency range introduces an additional uncertainty of $<0.1\%$ to the total $^3P_0^o$ polarizability.

It is worth mentioning that the core is the same for the $5s^2$ $^1S_0$ and the $5s5p\ ^3P_J^o$ states. For this reason,

$$\alpha_{^1S_0}^c(\omega) \approx \alpha_{^3P^o_J}^c(\omega)$$

and we arrive at the following expression:

$$\alpha_{^1S_0}(\omega) - \alpha_{^3P^o_J}(\omega) \approx \alpha_{^1S_0}^v(\omega) - \alpha_{^3P^o_J}^v(\omega). \quad (6)$$

The method of calculation for the dynamic valence polarizabilities $\alpha^v(\omega)$ is described elsewhere (see, e.g., Refs. [36,37]). Here we only briefly recapitulate its main features. These polarizabilities are computed with the Sternheimer [38] or Dalgarno-Lewis [39] method implemented in the CI+MBPT framework. [Here we denote Σ and RPA corrections as the many-body perturbation theory (MBPT) corrections.] Given the wave function and energy E_g of state g, we find intermediate-state wave functions $\delta\psi_\pm$ from an inhomogeneous equation

$$|\delta\psi_\pm\rangle = \frac{1}{H_{\text{eff}}-(E_g\pm\omega)}\sum_k |k\rangle\langle k|d_0|g\rangle$$

$$= \frac{1}{H_{\text{eff}}-(E_g\pm\omega)}d_0|g\rangle. \quad (7)$$

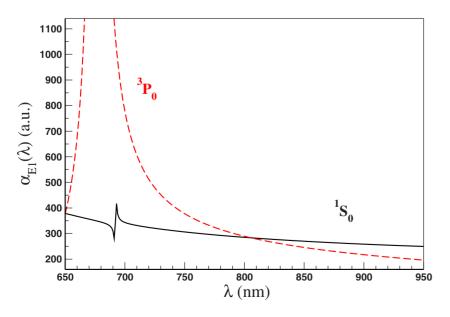Using Eq. (4) and $\delta\psi_\pm$ introduced above, we obtain

TABLE II. Calculated polarizabilities at a few selected optical wavelengths. Wavelengths λ are in nm, the frequencies ω are in a.u. and the electric dipole ac polarizabilities of the $5s^2\ ^1S_0$ and the $5s5p\ ^3P_{0,1}^o$ states are in au. The polarizability of the $^3P_1^o$ state is calculated for the projection $|m_J|=1$ and linearly polarized light.

λ	ω	$\alpha(5s^2\ ^1S_0)$	$\alpha(5s5p\ ^3P_0^o)$	$\alpha(5s5p\ ^3P_1^o)$
	0.0000	197.2	457.0	498.8
698.4	0.0652	351.8	909.2	
805.0	0.0566	288.9	289.3	
813.4	0.0560	286.0	280.5	
902.2	0.0505	263.5		263.4
914.0	0.0499	261.2		256.1

$$\alpha^v(\omega) = \frac{1}{2}(\langle g|d_0|\delta\psi_+\rangle + \langle g|d_0|\delta\psi_-\rangle), \qquad (8)$$

where superscript v emphasizes that only excitations of the valence electrons are included in the intermediate-state wave functions $\delta\psi_\pm$ due to the presence of H_{eff}.

In Table II we present the values of the static polarizabilities and the ac polarizabilities of the $5s^2\ ^1S_0$ and the $5s5p$ $^3P_{0,1}^o$ states computed for different values of λ using the CI+MBPT approach. As a first step we solved an inhomogeneous equation and found the valence parts of the polarizabilities. Then the values of the polarizabilities of the ground state were corrected as follows. We used the fact that the intermediate $5s5p\ ^1P_1^o$ state contributes to this polarizability at the level of 97%. Knowing the experimental energy difference $(E_{^1P_1^o}-E_{^1S_0})$ and the matrix element $|\langle 5s^2\ ^1S_0\|d\|5s5p\ ^1P_1^o\rangle|=5.249(2)$ a.u. extracted from the precise measurement of the lifetime of the $5s5p\ ^1P_1^o$ state [16], we replaced the theoretical contribution of the $5s5p\ ^1P_1^o$ state to the ground-state polarizability by the experimental value. Finally, we added α^c term to the valence parts, arriving at the values listed in Table II.

Starting from the 0.05% uncertainty of the $|\langle 5s^2\ ^1S_0\|d\|5s5p\ ^1P_1^o\rangle|$ matrix element, we estimated the uncertainty of the a.c. polarizability of the ground state at the level of 0.1%. In particular, for the static polarizability, we obtained $\alpha_{^1S_0}(0)=197.2$ a.u., in perfect agreement with the result obtained in Ref. [15] using a different basis set.

Experiments [8,34] have determined the magic wavelengths for the $^1S_0$-$^3P_0^o$ and $^1S_0$-$^3P_1^o(m_J=\pm 1)$ transitions to be 813.4 and 914 nm, respectively. As is seen from Table II, the calculations carried out in this work give the values of 805 and 902 nm for these magic wavelengths, respectively. Thus, the agreement between theoretical and experimental results is at the level of 1%. The behavior of the ac polarizabilities of the $^1S_0$ and the $^3P_0^o$ states in the wavelength range from 650–950 nm is illustrated in Fig. 2. A large peak at 679 nm for the $^3P_0^o$ state arises from the contribution of the $5s6s\ ^3S_1$ state, while a small peak in the vicinity of 690 nm for the $^1S_0$ ac polarizability is due to the contribution of the $5s5p\ ^3P_1^o$ state. Experimentally, the differential ac polarizabilities in the form of the clock frequency shift induced by the clock probe laser itself is known. With a probe laser intensity of 20 mW/cm^2, the fractional frequency shift was measured to be $-1.5(0.4)\times 10^{-15}$ [8]. Assuming the same probe laser intensity and the values of the polarizabilities for the $^1S_0$ and $^3P_0^o$ states obtained at 698.4 nm (see Table II), the calculated fractional shift is -1.2×10^{-15}, in a good agreement with the experimental value.

It is worth noting that knowing the precise experimental values of the magic wavelengths and using the fact that $\alpha_{^3P_0^o}(813.4\text{ nm})=\alpha_{^1S_0}(813.4\text{ nm})$ and $\alpha_{^3P_1^o,|m_J|=1}(914\text{ nm})=\alpha_{^1S_0}(914\text{ nm})$, we can refine our calculation and predict with high accuracy the values of the ac polarizabilities of the $^3P_0^o$ and $^3P_1^o$ states at these wavelengths. We obtain $\alpha_{^3P_0^o}(813.4\text{ nm})=286.0(3)$ a.u. and $\alpha_{^3P_1^o,|m_J|=1}(914\text{ nm})=261.2(3)$ a.u., matching the polarizabilities of the $^1S_0$ state at these two wavelengths.

In Table III we present the values of the individual contributions from six low-lying even-parity intermediate states to the valence parts of the static polarizability and the ac

FIG. 2. (Color online) Electric dipole ac polarizabilities for $5s^2$ $^1S_0$ (solid line) and $5s5p\ ^3P_0$ (dashed line) states of Sr. The polarizabilities are shown as a function of optical wavelength λ.

TABLE III. Individual contributions (ICs) from six low-lying intermediate states to the valence parts of the static polarizability $\alpha^v_{3P^o_0}(0) = 451.5$ a.u. and to the ac polarizabilities (in a.u.) at the wavelengths $\lambda = 813.4$ and 698.4 nm. $\alpha^v_{3P^o_0}(813.4 \text{ nm}) = 280.6$ a.u. and $\alpha^v_{3P^o_0}(698.4 \text{ nm}) = 903.8$ a.u. $D \equiv |\langle 5s5p\,^3P^o_0\|d\|n\rangle|$ is the reduced matrix element of the electric dipole operator **d**. The row "total" gives the sum of the contributions for each column.

$|n\rangle$	D (a.u.)	IC to $\alpha^v_{3P^o_0}(0)$		IC to $\alpha^v_{3P^o_0}(813.4 \text{ nm})$		IC to $\alpha^v_{3P^o_0}(698.4 \text{ nm})$	
		(a.u.)	(%)	(a.u.)	(%)	(a.u.)	(%)
$5s4d\,^3D_1$	2.74	286.1	63.4	−31.0	−11.3	−22.2	−2.5
$5s6s\,^3S_1$	1.96	38.3	8.5	126.4	45.9	705.8	78.1
$5s5d\,^3D_1$	2.50	44.2	9.8	68.3	24.8	84.8	9.4
$5p^2\,^3P_1$	2.56	45.3	10.0	68.7	25.0	84.1	9.3
$5s7s\,^3S_1$	0.52	1.7	0.4	2.4	0.9	2.8	0.3
$5s6d\,^3D_1$	1.13	7.4	1.6	9.6	3.5	10.8	1.2
Total		423.4	93.8	245.8	89.3	868.4	96.1

polarizabilities at $\lambda = 813.4$ nm and $\lambda = 698.4$ nm for the $^3P^o_0$ state. As is seen from Table III, for the $^3P^o_0$ static polarizability, four even-parity states ($5s4d\,^3D_1$, $5s6s\,^3S_1$, $5s5d\,^3D_1$, and $5p^2\,^3P_1$) contribute at the level of 92%. If the sum of these four contributions are determined experimentally with an accuracy $\sim 0.1\%$ and the contributions of all the rest of the discrete and continuum states are known at the level of 1–2%% from calculations, the overall polarizability of the $5s5p\,^3P^o_0$ state can be determined with the accuracy $\sim 0.1\%$.

Experimental determination of the four dominant contributions may be accomplished directly from lifetime or transition rate measurements. However, the lifetime data should be accompanied by high accuracy branching ratio measurements. Alternatively, we could measure single channel decay directly to the $5s5p\,^3P^o_0$ state. In addition, it is possible to constrain the four contributions using other spectroscopic data such as the magic wavelength λ_0 and the light shift at 698 nm, which will naturally be measured and confirmed by a number of future clock experiments. At both wavelength regions the same four states dominate the polarizability as in the static case. The general strategy would be to use spectroscopic data to constrain the most dominant contribution for that specific case.

Since the $5s4d\,^3D_1$ state dominates the four critical contributions to the static polarizability, and has less contribution to the dynamic polarizability at wavelengths of interest (see Table III), it would thus be maximally beneficial to measure this contribution directly with an oscillator strength measurement between $5s5p\,^3P^o_0$ and $5s4d\,^3D_1$. Doing so avoids upscaling of the uncertainty via error propagation. The high accuracy experimental measurement for the $5s5d\,^3D_1$ state [50] can be further improved by monitoring its decay to $5s5p\,^3P^o_0$ directly. Then, combining the measurements of λ_0 and the light shift at 698 nm would allow us to constrain contributions from both $5s6s\,^3S_1$ and $5p^2\,^3P_1$, permitting constraining $\alpha_{3P^o_0}(0)$ at the level of $\alpha_{1S_0}(0)$.

The magic wavelength, λ_1, could in principle also aid the constraint. However, additional sensitivities of the $5s5p\,^3P^o_1$ polarizability from $J=0$ and $J=2$ even-parity states are large

and complex. Furthermore, the vector nature of this state requires careful experimental control of light polarization. In the following section we present the results of the theoretical calculation of transition rates and oscillator strengths most relevant to the $^3P^o_0$ and $^1S_0$ polarizabilities and compare them to existing experimental and theoretical data in the literature.

D. Transition rates and oscillator strengths

The transition rate (W) and the oscillator strength (f) for a transition from an initial state $|\gamma'J'L'S'\rangle$ to a final state $\langle\gamma JLS|$ can be represented as (see, e.g., Ref. [40])

$$W(\gamma'J'L'S' \rightarrow \gamma JLS)$$
$$= \frac{4(\omega\alpha)^3}{3}\frac{1}{2J'+1}|\langle\gamma JLS\|d\|\gamma'J'L'S'\rangle|^2, \quad (9)$$

$$f(\gamma'J'L'S' \rightarrow \gamma JLS) = -\frac{2\omega}{3}\frac{1}{2J'+1}|\langle\gamma JLS\|d\|\gamma'J'L'S'\rangle|^2, \quad (10)$$

where γ denotes all quantum numbers other than J, L, and S, and $\omega = E_{\gamma'J'} - E_{\gamma J}$ is the transition frequency from the initial state to the final state. With this definition the oscillator strength is positive for absorption and negative for emission.

Using Eqs. (9) and (10) and knowing $E1$ transition amplitudes between different states, we were able to calculate rates and oscillator strengths for the transitions involving the $5s^2\,^1S_0$ and the $5s5p\,^3P^o_0$ states. In Table IV we list the transition rates and oscillator strengths for the strongest transitions from the mentioned states. Note that the transition rates $W_{n \rightarrow {}^1S_0,\,{}^3P^o_0}$ and the oscillator strengths $f_{{}^1S_0,\,{}^3P^o_0 \rightarrow n}$ were calculated with use of the theoretical energy levels. Where available we compare our results with other experimental and theoretical values. As is seen from Table IV, there is a reasonable agreement between the results of this work and other data.

In certain cases we used for comparison the nonrelativistic values of transition rates given in the literature. In the LS

TABLE IV. Transition rates $W_{n\to 0}$ and oscillator strengths $f_{0\to n}$ for relevant energy levels in Sr. The results are compared with other available experimental and theoretical data.

| | | $W_{n\to 0}(\times 10^6 \text{ s}^{-1})$ | | $f_{0\to n}$ | |
$\langle 0|$	$|n\rangle$	This work	Other data	This work	Other data[a]
$5s^2 \, ^1S_0$	$5s5p \, ^1P_1^o$	186.0[b]	190.01(14)[c]	1.82[b]	1.92(6)
			191.6(1.1)[d]		
			215[e]		
	$5s6p \, ^1P_1^o$	1.49	1.87(26)[a]	0.0058	0.0072(10)
			3.79[e]		
	$5s7p \, ^1P_1^o$	5.13	5.32(61)[a]	0.15	0.16(2)
			3.19[e]		
$5s5p \, ^3P_0^o$	$5s4d \, ^3D_1$	0.29		0.088	
	$5s6s \, ^3S_1$	8.39	7.32[e]	0.173	
	$5s5d \, ^3D_1$	38.1	30.7[e]	0.395	
	$5p^2 \, ^3P_1$	41.3		0.418	
	$5s7s \, ^3S_1$	2.28	1.80[e]	0.019	
	$5s6d \, ^3D_1$	14.3		0.099	

[a]Parkinson *et al.* [43] (expt.).
[b]These values are presented only for comparison. In all calculations performed in this work involving $\langle ^1S_0\|d\|^1P_1^o\rangle$, we used the value of this ME obtained from Ref. [16].
[c]Yasuda *et al.* [16] (expt.).
[d]Nagel *et al.* [44] (expt.).
[e]These numbers were obtained from the values given in Werij *et al.* [41] with use of Eqs. (9) and (11) (see Sec. III D for details).

coupling approximation, there is a simple relation between relativistic and nonrelativistic reduced matrix elements (MEs) of the operator **d**. Since the operator **d** commutes with **S** we obtain [40]

$$\langle \gamma JLS\|d\|\gamma'J'L'S'\rangle = \delta_{SS'}\sqrt{(2J+1)(2J'+1)}$$
$$\times (-1)^{S+L+J'+1}\begin{Bmatrix} L & J & S \\ J' & L' & 1 \end{Bmatrix}$$
$$\times \langle \gamma LS\|d\|\gamma'L'S\rangle. \quad (11)$$

Knowing a nonrelativistic transition rate we were able to determine the corresponding ME of the electric dipole operator $\langle \gamma LS\|d\|\gamma'L'S\rangle$. If the LS coupling approximation is valid, using Eq. (11), the nonrelativistic ME can be related to the relativistic ME $\langle \gamma JLS\|d\|\gamma'J'L'S'\rangle$. We also need to account for the fact that in a nonrelativistic case the transition frequency ω_{LS} between two states is given by expression $\omega_{LS}=\overline{E_{\gamma'J'L'S'}}-\overline{E_{\gamma JLS}}$, where $\overline{E_{\gamma JLS}}$ is the center of gravity of the respective multiplet. For this reason, in general, ω_{LS} can slightly differ from $\omega=E_{\gamma'J'}-E_{\gamma J}$. Finally, using Eq. (9) we can find the relativistic transition rate. We used this approach to compare the relativistic transition rates obtained in this work with the nonrelativistic values presented in Ref. [41].

If the LS coupling breaks down, Eq. (11) is no longer valid. In this case, to compare the relativistic transition rates given by Eq. (9) with the non-relativistic transition rates $W(\gamma'L'S'\to\gamma LS)$, one should use a more general relation [40]

$$W(\gamma'L'S' \to \gamma LS) = \frac{1}{(2L'+1)(2S'+1)}$$
$$\times \sum_{JJ'}(2J'+1)W(\gamma'J'L'S' \to \gamma JLS). \quad (12)$$

In the right-hand side of this equation the summation goes over all possible values of J' and J. Consequently, we need to find all transitions rates (permitted by selection rules) from the fine structure levels of one multiplet to the fine structure levels of another multiplet.

To provide a straightforward comparison of the calculation here with experimental data, lifetimes of the four states which dominate the $^3P_0^o$ polarizability contributions have been evaluated. For these four states, decay to the $5s5p \, ^3P_J^o$ states is the only significant radiative decay channel so the lifetimes can provide direct information on the relevant matrix elements. A number of lifetime and transition rate measurements are available for comparison [41,42,45–52], however in many instances with limited accuracy. Table V summarizes the results where the $5s4d \, ^3D_1$, $5s6s \, ^3S_1$, $5s5d \, ^3D_1$, and $5p^2 \, ^3P_1$ lifetime calculations are compared to available measurements. In some cases, the measured lifetimes were reported for a particular J value in the excited state multiplet, and in others only a mean lifetime for the entire multiplet was given, leading to complications in the analysis.

TABLE V. Experimental lifetime data for the low-lying even-parity states. Theory values calculated in this work are provided for comparison. $\overline{^3D}$ denotes measurement of the ^3D manifold without definitive angular momenta.

Excited state	τ (ns)	This work
$5s4d\ ^3D_1$		2040
$\overline{^3D}$	2900(200)[a]	2400[b]
	4100(600)[c]	
$5s6s\ ^3S_1$	15.0(8)[d]	14.1
	10.9(1.1)[e]	
	12.9(7)[f]	
$5s5d\ ^3D_1$	16.49(10)[g]	16.9
$^3D_2$	16.34(13)[g]	16.8
$^3D_3$	16.29(24)[g]	
$\overline{^3D}$	17.1(8)[h]	
	16.0(6)[d]	
	16.7(1.0)[f]	
$5p^2\ ^3P_0$		7.8
$^3P_1$	8.3(0.4)[d]	7.6
	8.8(1.2)[e]	
	10.2(2.4)[i]	
$^3P_2$	7.89(05)[g]	7.9
	7.8(1.8)[e]	
	8.3(0.4)[d]	

[a]Reference [42].
[b]This value is calculated using Eq. (12).
[c]Reference [45].
[d]Reference [46].
[e]Reference [47].
[f]Reference [48].
[g]Reference [50].
[h]Reference [49].
[i]Reference [51].

In the case of the $5s4d\ ^3D$ state we also evaluated the total transition rate for the multiplet since to our knowledge the only lifetime measurements for the $5s4d\ ^3D$ levels were performed on the entire multiplet. In the framework described above we found the $W(5s4d\ ^3D_{J'} \rightarrow 5s5p\ ^3P_J^o)$ transition rates for all possible J and J', and using Eq. (12), we obtained

$$\frac{1}{15}\sum_{JJ'}(2J'+1)W(5s4d\ ^3D_{J'} \rightarrow 5s5p\ ^3P_J^o) = 0.41 \times 10^6\ \text{s}^{-1}$$

in agreement with the experimental value $W(5s4d\ ^3D \rightarrow 5s5p\ ^3P^o) = 0.345(24) \times 10^6\ \text{s}^{-1}$ [42].

The lifetimes of the $5s5d\ ^3D_J$ states have been measured with high accuracy (0.1%) in Ref. [50] and are in good agreement with other measurements as well as our calculated values. Reference [50] also reported a 1% measurement of the $5p^2\ ^3P_2$ lifetime, while other direct measurements of this

multiplet yield consistent $^3P_1$ lifetimes having accuracies at the 15–20% level. Relative to $5s5d\ ^3D_J$ and $5p^2\ ^3P_J$, the $5s6s\ ^3S_1$ experimental data has larger scatters between different measurements. Notably all of these measured lifetime values agree well with our calculations.

Given the results in Tables V and III, the $5s4d\ ^3D_1$ state should have the highest measurement priority as it dominates the $^3P_0^o$ static polarizability. It also has a large disagreement between the experiments in Refs. [42,45], meriting further experimental investigations. The next priority goes to the $5s6s\ ^3S_1$ state due to the scatter in existing data and its large contribution to the ac polarizability of $^3P_0^o$. Perhaps a good strategy is to measure its decay directly to individual $5s5p\ ^3P_J^o$ states. Confirmation of the high accuracy result of Ref. [50] for the $5s5d\ ^3D_1$ state and improvement upon the $5p^2\ ^3P_1$ result listed in Table V or, alternatively, the use of the measured magic wavelength and clock laser light shift, can then be sufficient to determine the $^3P_0^o$ polarizability at the 0.1% level.

IV. CONCLUSION

In this work we have performed detailed calculations for further reducing the inaccuracy of the Sr optical atomic clock to 1×10^{-17} and below. To focus on the outstanding problem of BBR-related frequency shifts, we calculated ac polarizabilities of the $^1S_0$ and $^3P_0^o$ clock states. We verify our calculations with available experimental data. For example, the theoretically calculated magic wavelengths for the $^1S_0$-$^3P_0^o$ and the $^1S_0$-$^3P_1^o$ transitions are in 1% agreement with experiments. The agreement between theory and experiment on the ac Stark shift of the clock transition itself is also good. We have calculated individual contributions of six lowest-lying even-parity states to the polarizability of the $^3P_0^o$ state at $\omega = 0$ and for the wavelengths $\lambda = 698.4$ nm and 813.4 nm. We determined four even-parity states whose total contribution to the static polarizability of the $^3P_0^o$ clock state is $\sim 90\%$. Using the modern methods of atomic calculations we can find the contribution of all the other discrete and continuum states (constituting 10%) to the $^3P_0^o$ polarizability at the level of 1–2%%. For this reason, if the contributions of the four states identified here are experimentally determined with 0.1% accuracy, the same level of accuracy can be obtained for the total polarizability of $^3P_0^o$. In the near future we plan to undertake experimental measurements to determine the oscillator strengths for the four identified states. Measurements could include transition linewidths, power broadening coefficients, direct lifetime determinations of individual J levels, and improved determination of the clock laser ac Stark shifts. These experimental measurements can be further combined with the well-known value of λ_0. The experimentally determined values will be used to refine the theory calculations presented here to reach the goal of determining the polarizability of $^3P_0^o$ at 0.1%.

[1] H. Katori, M. Takamoto, V. G. Palchikov, and V. D. Ovsiannikov, Phys. Rev. Lett. **91**, 173005 (2003).

[2] A. D. Ludlow, M. M. Boyd, T. Zelevinsky, S. M. Foreman, S. Blatt, M. Notcutt, T. Ido, and J. Ye, Phys. Rev. Lett. **96**, 033003 (2006).

[3] M. M. Boyd, A. D. Ludlow, S. Blatt, S. M. Foreman, T. Ido, T. Zelevinsky, and J. Ye, Phys. Rev. Lett. **98**, 083002 (2007).

[4] G. K. Campbell *et al.*, e-print arXiv:physics/0804.4509.

[5] R. Le Targat, X. Baillard, M. Fouche, A. Brusch, O. Tcherbakoff, G. D. Rovera, and P. Lemonde, Phys. Rev. Lett. **97**, 130801 (2006).

[6] X. Baillard *et al.*, Eur. Phys. J. D **48**, 11 (2008).

[7] M. Takamoto *et al.*, J. Phys. Soc. Jpn. **75**, 104302 (2006).

[8] A. D. Ludlow *et al.*, Science **319**, 1805 (2008).

[9] N. Poli *et al.*, Phys. Rev. A **77**, 050501(R) (2008).

[10] J. Ye, H. J. Kimble, and H. Katori, Science **320**, 1734 (2008).

[11] M. M. Boyd *et al.*, Science **314**, 1430 (2006).

[12] S. G. Porsev and A. Derevianko, Phys. Rev. A **69**, 042506 (2004).

[13] R. Santra, K. V. Christ, and C. H. Greene, Phys. Rev. A **69**, 042510 (2004).

[14] M. M. Boyd, T. Zelevinsky, A. D. Ludlow, S. Blatt, T. Zanon-Willette, S. M. Foreman, and J. Ye, Phys. Rev. A **76**, 022510 (2007).

[15] S. G. Porsev and A. Derevianko, Phys. Rev. A **74**, 020502(R) (2006).

[16] M. Yasuda, T. Kishimoto, M. Takamoto, and H. Katori, Phys. Rev. A **73**, 011403(R) (2006).

[17] I. P. Grant and H. M. Quiney, Adv. At. Mol. Phys. **23**, 37 (1988).

[18] S. A. Kotochigova and I. I. Tupitsin, J. Phys. B **20**, 4759 (1987).

[19] P. Jönsson and C. Froese Fischer, Phys. Rev. A **50**, 3080 (1994).

[20] V. A. Dzuba, V. V. Flambaum, and M. G. Kozlov, Phys. Rev. A **54**, 3948 (1996).

[21] V. A. Dzuba, M. G. Kozlov, S. G. Porsev, and V. V. Flambaum, Zh. Eksp. Teor. Fiz. **114**, 1636 (1998) [J. Exp. Theor. Phys. **87**, 885 (1998)].

[22] S. G. Porsev, Yu. G. Rakhlina, and M. G. Kozlov, Phys. Rev. A **60**, 2781 (1999).

[23] S. G. Porsev, Yu. G. Rakhlina, and M. G. Kozlov, J. Phys. B **32**, 1113 (1999).

[24] D. Kolb, W. R. Johnson, and P. Shorer, Phys. Rev. A **26**, 19 (1982).

[25] W. R. Johnson, D. Kolb, and K.-N. Huang, At. Data Nucl. Data Tables **28**, 333 (1983).

[26] M. G. Kozlov and S. G. Porsev, Opt. Spectrosc. **87**, 384 (1999) [Opt. Spektrosk. **87**, 352 (1999)].

[27] V. F. Brattsev, G. B. Deineka, and I. I. Tupitsyn, Izv. Akad. Nauk SSSR, Ser. Fiz. **41**, 2655 (1977) [Bull. Acad. Sci. USSR, Phys. Ser. (Engl. Transl.) **41**, 173 (1977)].

[28] P. Bogdanovich and G. Žukauskas, Sov. Phys. Collect. **23**, 13 (1983).

[29] C. E. Moore, *Atomic Energy Levels*, NBS, National Standards Reference Data Series No. 35 (U.S. GPO, Washington, DC, 1971), Vols. I-III.

[30] W. H. Oskay *et al.*, Phys. Rev. Lett. **97**, 020801 (2006).

[31] Y. Te, Metrologia **40**, 24 (2003).

[32] E. Simon, P. Laurent, and A. Clairon, Phys. Rev. A **57**, 436 (1998).

[33] A. D. Cronin, J. Schmiedmayer, and D. E. Pritchard, e-print arXiv:0712.3703.

[34] T. Ido and H. Katori, Phys. Rev. Lett. **91**, 053001 (2003).

[35] A. Derevianko, W. R. Johnson, M. S. Safronova, and J. F. Babb, Phys. Rev. Lett. **82**, 3589 (1999).

[36] S. G. Porsev and A. Derevianko, J. Chem. Phys. **119**, 844 (2003).

[37] M. G. Kozlov, S. G. Porsev, and V. V. Flambaum, J. Phys. B **29**, 689 (1996).

[38] R. M. Sternheimer, Phys. Rev. **80**, 102 (1950).

[39] A. Dalgarno and J. T. Lewis, Proc. R. Soc. London **233**, 70 (1955).

[40] I. I. Sobelman, *Atomic Spectra And Radiative Transitions* (Springer-Verlag, Berlin, 1979).

[41] H. G. C. Werij, C. H. Greene, C. E. Theodosiou, and A. Gallagher, Phys. Rev. A **46**, 1248 (1992).

[42] D. A. Miller, L. You, J. Cooper, and A. Gallagher, Phys. Rev. A **46**, 1303 (1992).

[43] W. H. Parkinson, E. M. Reeves, and F. S. Tomkins, J. Phys. B **9**, 157 (1976).

[44] S. B. Nagel, P. G. Mickelson, A. D. Saenz, Y. N. Martinez, Y. C. Chen, T. C. Killian, P. Pellegrini, and R. Côté, Phys. Rev. Lett. **94**, 083004 (2005).

[45] E. N. Borisov, N. P. Penkin, and T. P. Redko, Opt. Spektrosk. **63**, 475 (1987).

[46] G. Jönsson *et al.*, Z. Phys. A **316**, 255 (1984).

[47] U. Brinkmann, Z. Phys. **228**, 449 (1969).

[48] M. D. Havey, L. C. Balling, and J. J. Wright, J. Opt. Soc. Am. **67**, 488 (1977).

[49] A. L. Osherovich *et al.*, Opt. Spektrosk. **46**, 243 (1979).

[50] H. J. Andrä *et al.*, J. Opt. Soc. Am. **65**, 1410 (1975).

[51] W. Gornik, Z. Phys. A **283**, 231 (1977).

[52] K. Ueda, Y. Ashizawa, and K. Fukuda, J. Phys. Soc. Jpn. **51**, 1936 (1982).